Experimental evidence of Palladium dissolution in anodes for alkaline Direct Ethanol and Formate Fuel Cells

E. Berretti , M.V. Pagliaro , A. Giaccherini , G. Montegrossi , F. Di Benedetto , G.O. Lepore , F. D'Acapito , F. Vizza , A. Lavacchi

PII: S0013-4686(22)00513-8
DOI: https://doi.org/10.1016/j.electacta.2022.140351
Reference: EA 140351

To appear in: *Electrochimica Acta*

Received date: 9 November 2021
Revised date: 28 January 2022
Accepted date: 5 April 2022

Please cite this article as: E. Berretti , M.V. Pagliaro , A. Giaccherini , G. Montegrossi , F. Di Benedetto , G.O. Lepore , F. D'Acapito , F. Vizza , A. Lavacchi , Experimental evidence of Palladium dissolution in anodes for alkaline Direct Ethanol and Formate Fuel Cells, *Electrochimica Acta* (2022), doi: https://doi.org/10.1016/j.electacta.2022.140351

Experimental evidence of Palladium dissolution in anodes for alkaline Direct Ethanol and Formate Fuel Cells

E.Berretti[1], M. V. Pagliaro[1], A.Giaccherini[2], G.Montegrossi[3], F.Di Benedetto[4], G.O. Lepore[5], F. D'Acapito[6] , F. Vizza[1] and A. Lavacchi[1]

[1] Institute for the Chemistry of Organometallic Compounds, Italian National Research Council (ICCOM-CNR), 50019 Florence, Italy
[2] Chemistry Department, University of Florence, 50019 Florence, Italy
[3] Institute of Geosciences and Earth Resources, Italian National Research Council (IGG-CNR), 50121 Florence, Italy
[4] Department of Earth Sciences, University of Ferrara, 44122 Ferrara, Italy
[5] Earth Sciences Department, University of Florence, 50121 Florence, Italy
[6] Istituto di Officina dei Materiali, Italian National Research Council (IOM-CNR), c/o European Synchrotron Radiation Facility (ESRF), Grenoble, France

Keywords: Palladium, Electrocatalysis, Fuel Cells, Ethanol, Formate, X-Ray Absorption Spectroscopy

Abstract:

Palladium is one of the best anodic catalysts for Alkaline Direct Alcohol Fuel Cell (DAFC) applications. However, its adoption in Fuel Cells (FC) is still limited because of the deactivation of the catalyst, which hinders the long-term performance stability of the devices. In this article, we report the results of a Fixed Energy X-Ray Absorption Voltammetry (FEXRAV) investigation of a carbon-supported palladium electrocatalyst operating in a complete alkaline direct ethanol fuel cell (DEFC). Our results show palladium dissolution unambiguously, especially at cell polarizations corresponding to high anodic stresses. We have also investigated the behaviour of Pd electrocatalyst in a direct alkaline formate fuel cell (DFFC). Data show that when using formate as a fuel, the electrode Pd loss is negligible compared to the case of DEFC.

1. Introduction:

Direct alcohol fuel cells (DAFCs) are considered as a viable alternative for mid to low energy generation applications; these systems share average output electrical powers, together with low to no need of ancillaries for their duty cycles [1]. In this class of fuel cells, alcohol is fed in a liquid in the anodic compartment, while oxygen is supplied as gas in the cathodic compartment. The use of low-cost fuels, such as methanol, ethanol, glycerol and ethylene glycol, poses a significant advantage in the technological transfer of such devices[2]. These alcohols show a slight energy density difference in respect to fossil fuels [3,4] in their liquid form and can be produced "greenly" by fermentation of agricultural products and waste biomasses [5,6]. Moreover, the "direct" approach, which differs from the direct H_2 fuel cell and the reformer fuel cell approaches, permits the use of liquid alcoholic solutions to feed in the anodic compartment in ambient conditions, hindering all the risks related to the handling of high-pressure hydrogen reservoirs [7]. Among all the alcohol-fuelled cells, passive DAFCs represent a subclass geared toward portable application and low temperatures [8]. In these FCs, oxygen is usually delivered by the air to the cathode, while a static tank is used as a reservoir for the alcoholic fuel at the anode. This approach enhances the portability of this kind of cell, limiting their dimensions by eliminating the need for a flow system to the electrodes [9]. As a drawback, in the long-term runs, the depletion of the fuelling species from the solution could produce significant variations in the cell working potentials by modifying the mass transport, leading to faster degradation of the adopted catalysts.

In this context, platinum group metals (PGMs) are still considered the best electrocatalytic materials for the majority of the reactions (both cathodic and anodic) that can be exploited in low-temperature alcohol fuel

cells [10–14]. Due to PGMs cost and scarcity, the main challenge faced by researchers in the past few years was related to the decrease of precious metals loadings at the catalyst by maximising efficiency for both anodic and cathodic reactions. This objective was pursued by modifying the chemical nature of the catalysts (alloying PGM elements with less precious ones) [15,16] and/or by changing the catalyst architecture (novel nano-designs that maximize surface) [4,17]. Pt is still considered the prime choice catalyst for cathodic catalysts, while promising results were obtained with Porphyrin-like structures [18]. These M-N-C catalysts (M=Fe, Co) manifest a lower cost in respect to PGM catalysts (at the expense of lower durability) with no potential losses due to fuel crossover, thanks to their oxygen-selective nature. Oppositely, producing an effective anodic catalyst for alcohol electro-oxidation is still related to the adoption of PGMs [19]. Again, platinum is considered as the best catalyst for such reactions and is often employed in combination with Ruthenium [20] and other less noble metals, forming PtRuM [21–25] and PtRuMOx [26–28](M=Ti, V, Mn, W, Ni, Mo, etc.). Palladium, in respect to platinum, shows better activity towards alcohol oxidation in alkaline media [29,30], especially when in conjunction with CeO_2 [31,32] or Co [33]. The use of alkaline solutions could significantly improve FCs durability; indeed, the acidic environment is responsible for the degradation processes of the cells' structural components, the carbon support of the catalyst, and the ionic exchange membrane [34].

It has been shown that the main functional issue related to the use of Pd as anodic catalyst regards its deactivation, which leads to a loss in performance for palladium loaded DAFCs in alkaline media [35,36]. Studies have shown that palladium deactivation could occur by different pathways: a) nanoparticles coarsening (decrease in the electroactive area [37]), b) Formation of insoluble species on the surface [38–41], and c) Palladium dissolution [42,43]. These three effects could simultaneously contribute to the loss of cell performance to a certain extent, depending on the cell working potential and the fuel used [44,45]. Regarding alkaline Ethanol Oxidation Reaction (EOR) on Pd, initial evidence suggested that the fastest degradation mechanism is the one that leads to the formation of adhered species on the surface of the catalyst [40,41], which hinder fuel turnover. This phenomenon could indeed be responsible for loss in performances of palladium in the long run when it is subject to relatively low and constant potentials (below 0.6 V vs RHE). However, anode potential could vary widely in operative conditions in FC applications, exceeding palladium oxidation potential. Our previous experiments [46,47] at the European Synchrotron Radiation Facility (ESRF, BM-08 "LISA" CRG beamline), performed by stressing Pd/C nanoparticles in the 0 to 1.2 V vs RHE potential range using KOH 2M and KOH 2M + EtOH 2M electrolytes, highlighted loss in the electrochemical performances of the catalyst as a consequence of loss in palladium mass at the electrode. During these experiments, we used the Fixed Energy X-Ray Absorption Voltammetry technique (FEXRAV [48]) to uncover changes in the speciation of palladium. FEXRAV is particularly well versed in the study of the deactivation of metallic catalyst nanoparticles due to its elemental sensitivity. It is a mixed in-operando X-Ray Absorption Spectroscopy/Electrochemical technique that involves acquiring the x-ray absorption coefficient of an electrode subjected to electrochemical stimulus. During the acquisition, the X-Ray beam energy is held constant; the choice of the energy value is made by considering the maximum variation of the absorption coefficients of the species we expect to be formed at the target during electrochemical cycling. By setting the right X-ray beam energy it is then possible to determine the speciation of an element of choice, permitting the study of the transition between the metallic and ionic forms of a catalyst. By the use of the fuel cell we designed, FEXRAV enabled live characterization of both the variations between Pd^0 and Pd^{2+} at the electrode (by sampling the fluorescence x-ray signal), and of the Pd^{2+} present into solution (by the acquisition of the transmitted absorption x-ray coefficient). During our first experiments [46] we adopted a fixed beam energy of 24,370 keV (Figure 1-c). This value showed maximum $Pd^{2+}/Pd^{(0)}$ variation in the absorption coefficient (increase in μ by the increase of PdO). Results visible in Figure 1 demonstrated that, apart from local variations inside a single voltametric cycle (the valley-peak absorption coefficient variation in phase with the variation of potentials at the electrode), a constant loss of metallic palladium nanoparticles occurs in the long run (decrease in the overall absorption

signal μ) by formation of Pd^{2+} hydroxides into solution, when the electrode is subject to oxidative potentials for both alkaline and alkaline + ethanol electrolytes. A comparison between our results and computational speciation models [47] highlighted the presence of two main species in our system, $Pd^{(0)}$ and Pd^{2+} ($Pd(OH)_4^{2-}$), and only a minor amount of PdO as transient species at the electrode, thus confirming a dissolution pathway instead of a poisoning effect.

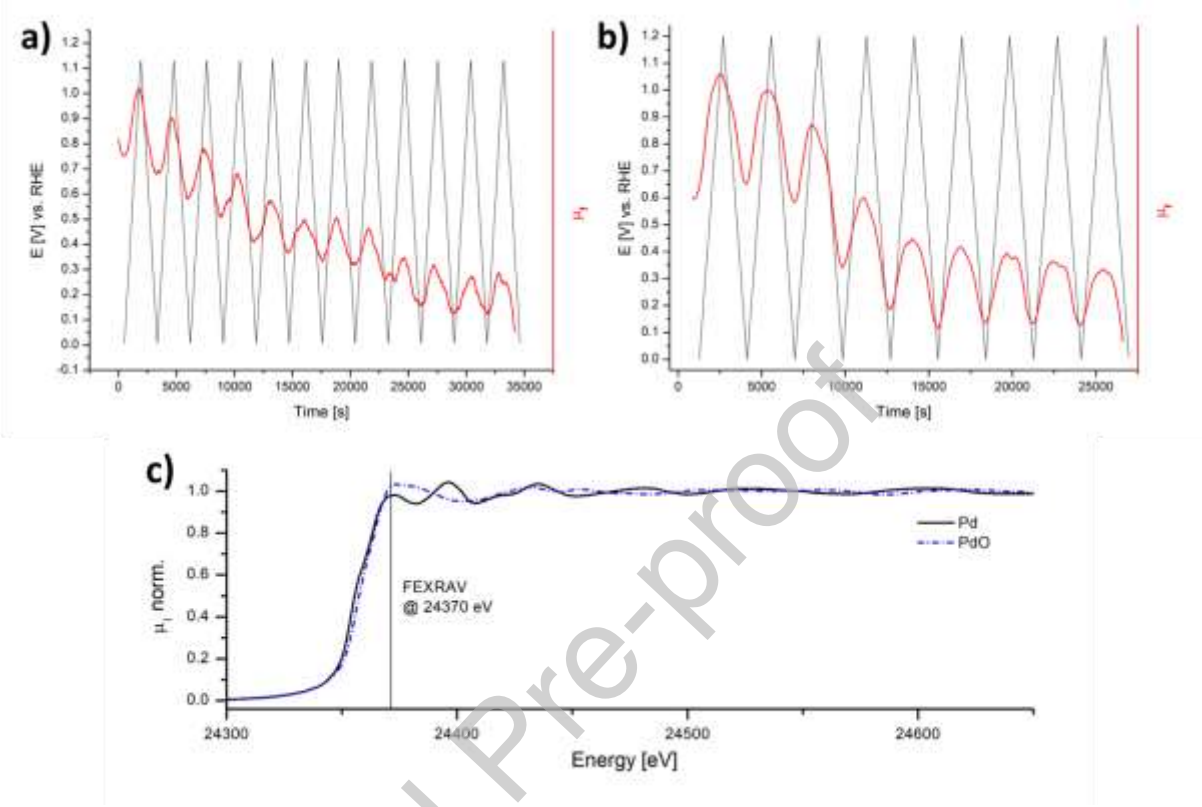

Figure 1 – Half-cell FEXRAV experiment: a) using KOH 2 M electrolyte and b) using KOH 2 M + EtOH 2 M electrolyte. The potential variation E at the electrode (black) and absorption coefficient derived from the fluorescence data (red) are reported vs time. c) XANES spectra of the Pd^0 and Pd^{2+} (PdO) standards, depicting variation between the two μ signals at 24370 eV.

We were then able to observe dissolution in the Pd/C catalyst in a half-cell set-up under high oxidative potentials. This situation was not completely representative in respect of the potentials the same catalyst could endure in a live fuel cell. The main purpose of this work is to investigate the behaviour of the same palladium catalyst in a complete FC, to check whether the same dissolution we observe in the half-cell experiments can be seen. With this study, we demonstrate the applicability of the FEXRAV technique to characterize complete fuel cells in-operando. In the article, we report the characterization of two complete Pd-based DAFCs by FEXRAV; a DEFC, for comparison with the half-cell experiments, and a DFFC. In addition, electrochemical characterization of the two fuel cells is also presented, to investigate the dissolution's influence on FC performances.

2. Experimental:

2.1. XAS Beamline Set-Up:

FEXRAV Experiments were conducted at the BM-08 LISA CRG Beamline [49] at the European Synchrotron Radiation Facility (ESRF) in Grenoble in the course of four experimental sessions (08-01-996, MA2936, MA3173, MA3431 and CH6101, in chronological order). A dynamically focusing sagittal monochromator equipped with a pair of Si (311) crystals was employed for the first three sessions. During experiment MA3431, samples were measured after the first part of the BM08 refurbishment using a pair of

flat Si [311] monochromator crystals. In all experimental sessions, a pair of Pt-coated mirrors ($E_{cutoff} \simeq 27$ keV for the first experimental sessions, $E_{cutoff} \simeq 40$ keV for MA3431) was used for harmonic rejection and vertical focusing on the sample; beam size on the sample was approximately 2000 µm (H) x 200 µm (V) [≃ 100 * 100 µm for MA3431]; energy resolution (ΔE/E) was ≈ 10^{-5}. Measurements were carried out in fluorescence mode, employing a 12-element solid-state (high purity Germanium) detector and transmission mode [50]. The beamline was equipped with ion chambers, one measuring the incoming beam (I_0) and the other reading beam transmitted through the sample (I_1) and a reference Pd foil (I_R). This particular setup permits both to avoid signal variations due to changes in the incoming photon beam (by simple normalization of the sample signal using I_0) and calibrate the acquisition energy through the simultaneous analysis of the reference.

Moreover, the I_1 gives information on the palladium present in the bulk of the solution in the form of solute Pd^{2+} ions. Finally, the fluorescence detector was placed on the side of the cell to collect the fluorescence signal coming mainly from the working electrode. A schematic view of the adopted experimental geometry can be found in Figure 2; it shows the top view of the electrochemical cell used for both Half-cell and Fuel Cell experiments, which was held in a 45° geometry concerning the incoming beam, enabling the acquisition of both I_f and I_1. ATHENA software package [51] was used to average multiple spectra and extract the normalised absorption edge.

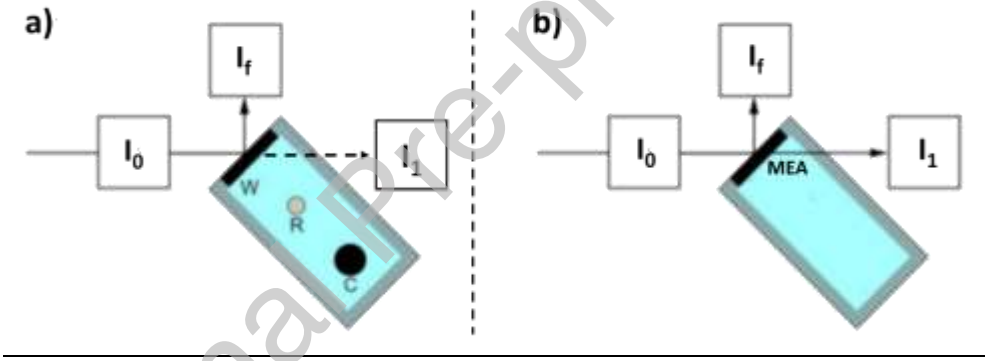

Figure 2 – Schematic top view of a) the Half-cell setup and b) the Fuel Cell setup during the synchrotron experiments. I_0 incident X-Ray Beam, I_1 transmitted X-Ray Beam, I_f Fluorescent signal. During initial half-cell experiments, only the I_f signal was sampled.

2.2. Electrochemical Set-Up:

2.2.1. FEXRAV experiments

A custom-made PMMA electrochemical cell was used for the synchrotron experiments on Fuel Cells (Figure 3-a). The cell was already used for half-cell experiments with minimal variations [46]. The cell design can be conceptually divided into two main parts, the head and the body. The head is responsible for the working electrode/MEA assembly (Figure 3-b). For Fuel Cell experiments, it is in between the adapter and the cell head that the MEA was mounted, as depicted in Figure 3-b. The head is responsible for the delimitation between the anodic part (the body) and the cathodic part (the outer environment, in contact with atmospheric O_2. Both Cell head and Adapter pieces have 5 mm holes enabling contact of the catalysts with the reactive species. . The body is composed of a central cylindrical shaft (10 ml) as an anodic reservoir for the electrolytic solution. Its volume was calculated to avoid substantial fuel concentration variation in the lifespan of a single experiment. The body also possesses various threaded holes, which enable the injection of different fluids in the working solution. A central thread is used to suspend the whole cell assembly to the motorized holder of the line to permit cell alignment to the beam. A PARSTAT 2263 potentiostat/galvanostat, programmed from the

control room, was adopted for the Synchrotron experiments. Two different solutions were used as electrolytes during the experiments: a) KOH 2M (Sigma-Aldrich) + EtOH 2M (Sigma-Aldrich) and b) KOH 2M (Sigma-Aldrich) + KCOOH 2M (Sigma-Aldrich). Solutions were prepared without disareation to simulate the expected conditions for an actual fuel cell during its working life. No catalyst loss into the bulk of the solution was noticed for both the half-cell and the fuel-cell experiments.

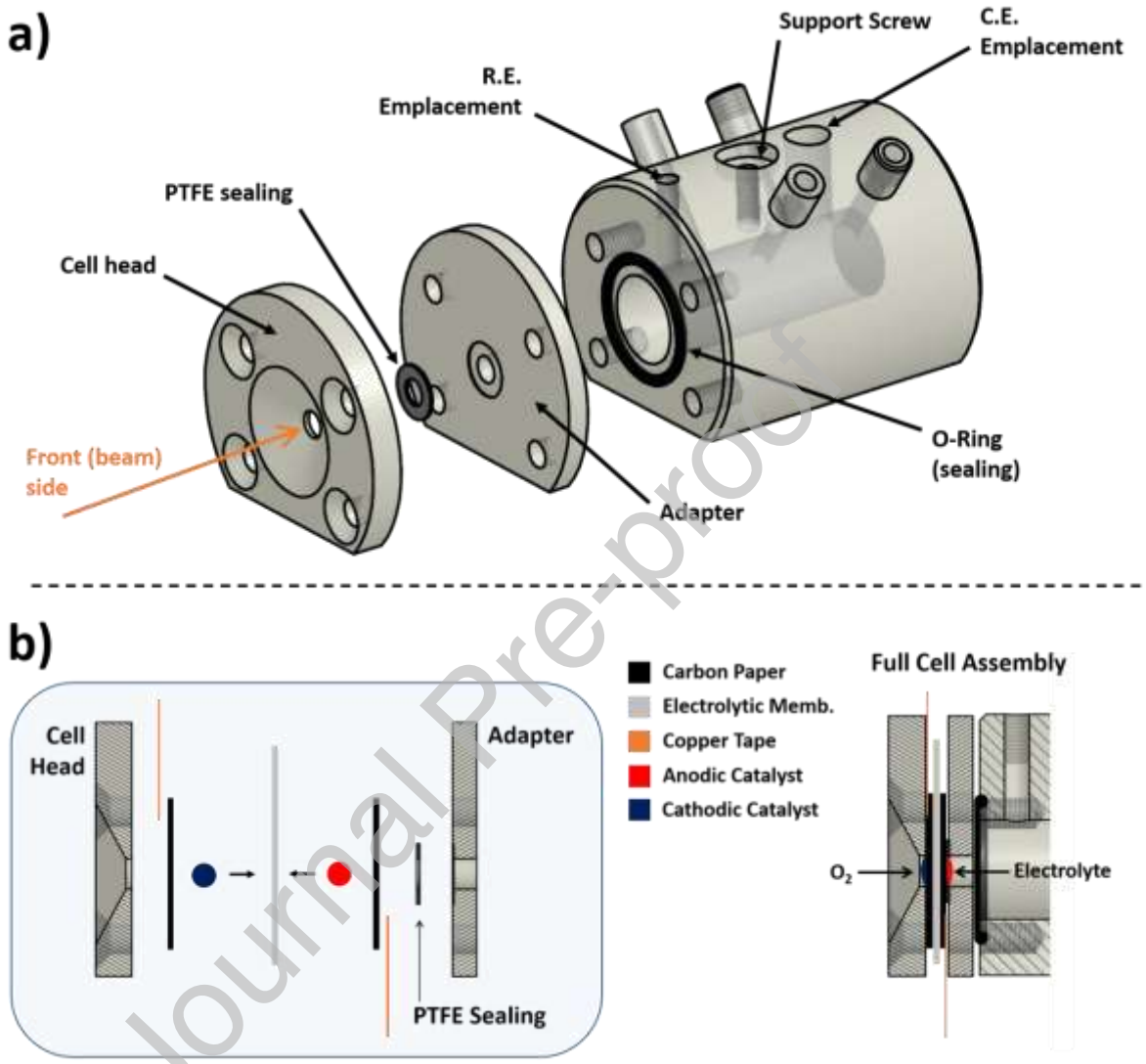

Figure 3 – a) Exploded view of the electrochemical cell. b) Exploded view of the fuel cell stack on the head assembly.

2.2.2. DAFCs performance experiments

The electrochemical cell was purchased from Scribner-Associates (USA). The MEAs (membrane electrode assemblies) were assembled by mechanically pressing together the cell hardware's anode, cathode, and membrane. The MEAs were composed of a nickel foam support coated with the Pd/C catalyst as the anode, a commercial Tokuyama A-006 anion-exchange membrane, and a FeCo/C catalyst supported on carbon cloth as the cathode. The cathode O_2 flow was regulated at 0.1 L min^{-1} using a Scribner 805e fuel cell station. The aqueous fuel solution (2 M KOH + 2 M ethanol or potassium formate) was delivered to the anode at 1 mL min^{-1}. The fuel cell performance was monitored with an ARBIN BT-2000 5A 4 channels instrument (Arbin Instruments, College Station, TX, USA). FCs experiments were recorded by applying a series of linear voltage ramps with a 10 mV s^{-1} scan rate (from OCP to 0.2 V for the formate cell, and from OCP to 0.1 V for the EtOH Cell, in order to visualize

the power curves peak completely) followed by a constant voltage step lasting 30 minutes (from 0.6 V to gradually lower values until 0.1 V) and 1 minute of rest, using a two-electrode configuration.

2.3. Catalysts:

A Pd/C nanoparticle catalyst was adopted as Working Electrode/anodic catalyst for Half-cell and Fuel Cell synchrotron experiments. It consisted of Pd nanoparticles, 5 nm in diameter, dispersed onto a carbon-black matrix in a weight ratio of 10%. Catalyst synthesis and characterization can be found in [52]. To be deposited on the inner part of the EC cell by drop-casting, the catalyst was mixed with NAFION ionomer, isopropanol and water in the 1:0.01:2:10 weight ratio and sonicated for 15 minutes. The drop-casting procedure led to an electrode Pd loading of 4 mg/cm^2 for fuel-cell experiments and 2 mg/cm^2 for half-cell OCP experiments.

For off-line performance experiments, the anode ink was prepared by mixing 100 mg of the previously cited catalyst with 100 mg of a 10% aqueous suspension of PTFE to form a dense catalyst paste; the paste is spread onto a 5 cm^2 Ni-foam support (Heze Tianyu Technology Development Co., China) to obtain a catalyst coated electrode with a Pd metal loading of 2 mg cm^{-2}.

A Fe-Co/C catalyst was used as the cathodic catalyst for the Fuel Cell FEXRAV and performance experiments. Its preparation and characterization can be found in [53]. To be used as the cathode, the catalyst was first mixed with a PTFE suspension and water to obtain a dense paste spread on a carbon cloth with a load of 2 mg/cm^2. The cathodic catalyst proven stability in the range of potentials and timespans explored in the present article; for this reason, no cathodic catalyst degradation was considered during fuel cell experiments [37,53].

Tokuyama A-006 was finally adopted as the membrane for the MEA assembly.

3. Results:

3.1. FEXRAV on Fuel cells

Two analogous DAFCs were assembled as described in the experimental part (2.2.2.). The first cell was fed with a KOH 2M + EtOH 2M solution, while the second one was fed by a KOH 2M + KCOOH 2M solution. The cells were left about 1 h to stabilize. After this period, Open Circuit Potential (OCP) was acquired between the anodic and the external cathodic leads (0,690 V for the EtOH FC, 0.852 V for the Formate FC). The cells were then mounted on the sample holder in the experimental hutch of the beamline and connected to the potentiostat in a two-electrode configuration. X-ray incident beam energy was fixed at a value of 24,370 keV. Cells were then cycled between their OCV and 0 V 13 times.

Data collected during these tests can be found in Figure 4 (EtOH FC) and Figure 5 (KCOOH FC), where the variation of cell potential in time is paired with the variation of the absorption coefficient for both the fluorescence (μ_f, red line) and transmitted (μ_1, blue line) signals. We were able to identify two types of variations in the absorption signals: an overall trend related to the variation μ from the beginning to the end of the experiment, and a single cycle variation, which takes into consideration the speciation inside the single voltammetric scan. The fluorescence signal obtained from the DEFC showed similar results in our previous half-cell experiments (Figure 1-b [46]). Its overall decrease after each voltammetric cycle was previously attributed to a decrease in palladium loading at the electrode (overall μ variation > single cycle $Pd^{2+}/Pd^{(0)}$ μ variation). This phenomenon is relevant if compared with the opposite trend of the transmitted signal, which was not considered in the previous half-cell experiments. Even if it is not possible to correlate the two sets of data quantitatively due to

experimental geometry, the transmitted signal can also sample part of the fuel solution, giving hints of the presence of palladium in the aqueous phase. Following the transmission detector signal, an increase in the overall μ between the cycles was noticeable. The opposite trends of the two μ can be explained only by the dissolution of the metallic palladium, which leaves the electrode in the form of soluble hydroxypalladiates into the bulk of the solution. A different trend was observed for the cell fuelled by potassium formate. It was still possible to notice a variation of the absorption signal due to the transition between $Pd^{(0)}$ and Pd^{2+} species for a single cycle. However, small to negligible variation was seen in the overall signal (in between the cycles) for both fluorescence and transmission μ's, suggesting no variation of the palladium loading at the electrode (overall μ variation << single cycle $Pd^{2+}/Pd^{(0)}$ μ variation), thus no long-term loss of palladium into the electrolyte due to dissolution.

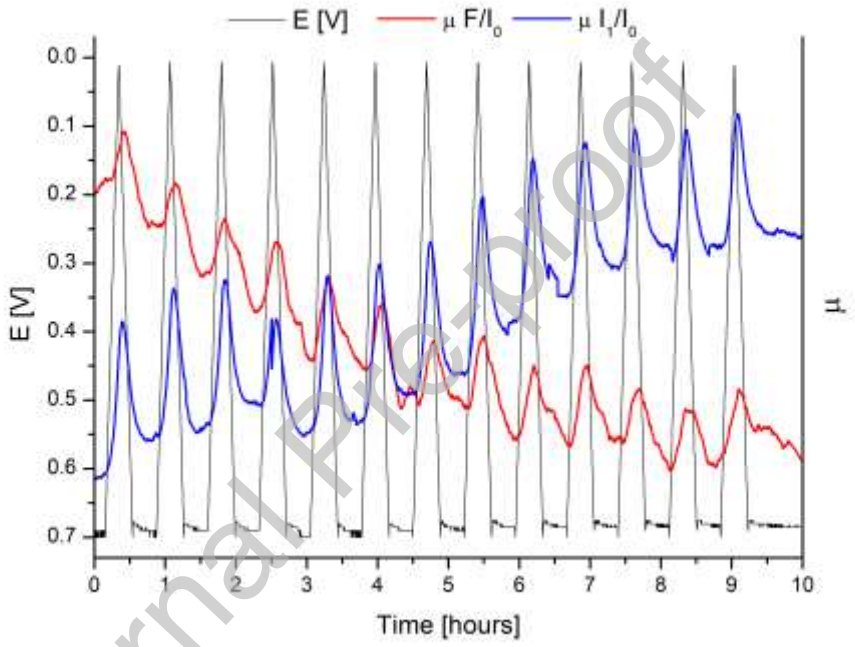

Figure 4 – FEXRAV cycles for the KOH 2 M + EtOH 2 M complete cell. The variation of the WE potential (black) is coupled in time with the variation of the X-Ray Absorption fluorescent signal (red) and the variation of the X-Ray Absorption transmitted signal (blue)

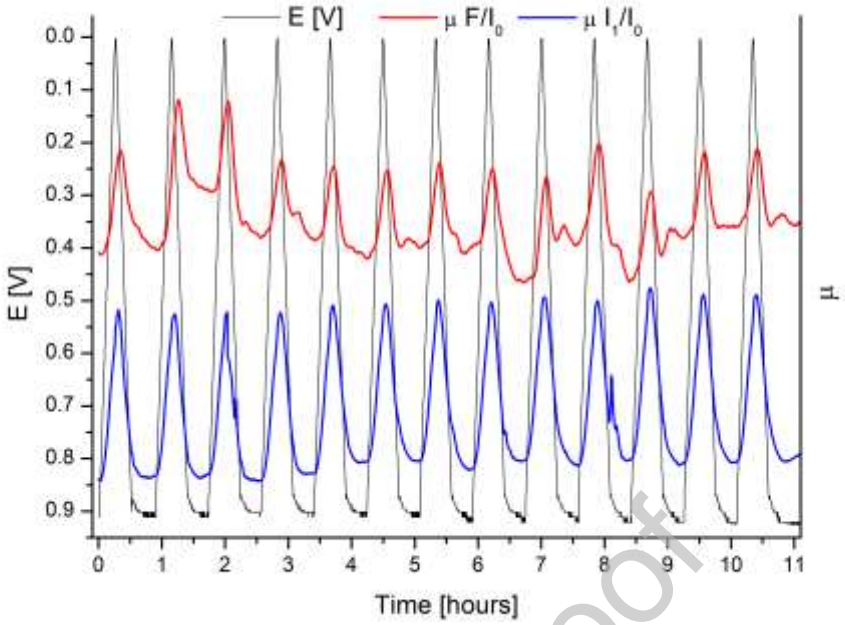

Figure 5 – FEXRAV cycles for the K Formiate 2 M + KOH 2 M complete cell. The variation of the WE potential (black) is coupled in time with the variation of the X-Ray Absorption fluorescent signal (red) and the variation of the X-Ray Absorption transmitted signal (blue)

For each FEXRAV cycle, potential values correspondent to the beginning of the transition between Pd^0 and Pd^{2+} were also collected (Figure 6). The definition of such potentials was paramount in order to mitigate palladium oxidation and dissolution. The values were obtained by extracting the potential values relative to the μ_f change in slope, just before the peak signal increase, for the forward voltametric scan in each FEXRAV cycle. E values were extracted from μ_f instead of μ_1; the increase in the transmitted absorption coefficient could in fact suffer from delay due to the palladium diffusion into solution. From Figure 6 we defined two safe potentials taken as the highest potentials from the plateau: 0.476 V for the DEFC, and 0.402 V for the DFFC (both the potentials are related to cathode vs. anode).

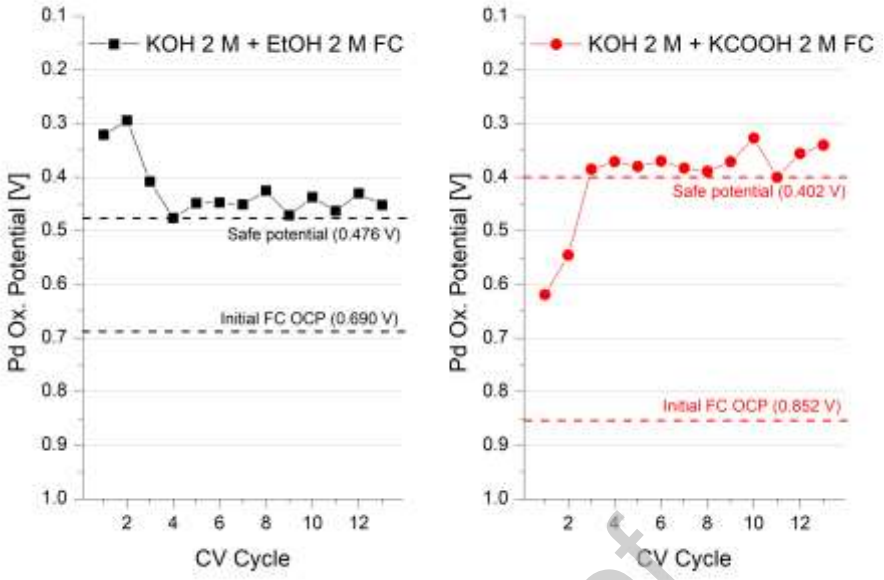

Figure 6 – Potentials related to the beginning of the oxidation of Pd for the DEFC (left) and DFFC (right)

To completely exclude the chemical dissolution of the catalyst in contact with the fuels, we acquired X-ray Absorption Near Edge Spectra (XANES) of the fresh catalyst in the half-cell experimental configuration during OCP. For this experiment, performed during the last beamtime, we used sodium salts (NaOH and NaCOOH from Sigma-Aldrich) instead of potassium ones to achieve lower x-ray attenuation from the electrolyte. Spectra were collected sequentially for about 4,5 hours. From each spectrum, the normalized absorption coefficient calculated from the transmission signal μ_1 at 24.370 keV was extracted, normalized by the value of the first spectra and plotted vs the time (Figure 7). This approach should detect an increase in the absorption coefficient in time with the decrease of palladium loading at the electrode. The choice of the half-cell setup fits well for the comparison with a whole fuel cell. In fact, from a thermodynamical point of view, the potential difference between electrodes in a FC during OCP should be equal to the difference between every single electrode in contact with its fuel. This is precisely the case for our half-cell experiment, in which the anodic catalyst is placed inside the cell, in contact with the same concentration of fuel + electrolyte. During the experiment, no variation of μ_1 in time outside the experimental uncertainty was recorded; at the same time, during FEXRAV experiments, a discrete variation of absorption coefficient has been seen, especially for ethanol electrolytes. The comparison between OCP and FEXRAV experiments confirmed that no spontaneous dissolution/oxidation of the catalyst occurs when the Pd/C is in contact with the two fuel solutions without applied potential. For the OCP experiments, variation in the μ is comparable with the experimental uncertainty.

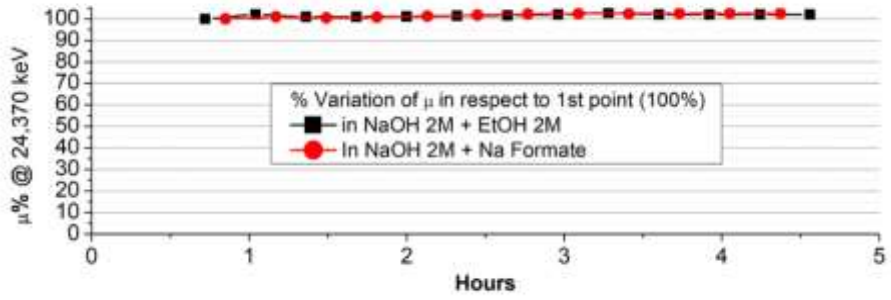

Figure 7 – Variation of the absorption coefficient (@ 24,370 keV) in time for the Pd/C catalyst during OCP in the three-electrode cell configuration. The value of the first point was taken as 100% (initial catalyst load), percentages of all the subsequent points are taken in respect to this value.

3.2. Fuel Cells Performance degradation

Power curves for both DEFC (KOH 2M + EtOH 2M) and DFFC (and KOH 2M + KCOOH 2M) were acquired after potentiostatic cycles at increasingly harmful polarizations. This different approach regarding dynamic potential cycling used in FEXRAV was meant to investigate potential-dependent changes in the FC performance in light of the catalyst dissolution. Once prepared, the cells were left to stabilize for about one hour to reach a steady OCP between cathode and anode (0.709 V for the Ethanol cell, 0.954 V for the formate cell). After the stabilization period, we acquired linear sweep voltammetry, followed by a 30 minutes potentiostatic cycle and a final 1-minute rest at the OCP. This measurement block was repeated six times for each cell, decreasing the potential by a 0.1 V factor for each subsequent potentiostatic cycle (0.6 V, 0.5 V, 0.4 V, 0.3 V, 0.2 V and 0.1 V between electrodes). This was made in order to stress the anodic catalyst even further with each subsequent potentiostatic cycle. A last linear sweep voltammetry was acquired after the 0.1 V potentiostatic procedure.

The analysis of the power curves extracted from the linear sweeps (Figure 8) gives a better understanding of the FCs loss in performance. In the ethanol FC (Figure 8-a), power curves peaks constantly decrease after each potentiostatic scan, reaching a steady-state after the 0.2 V step. For the DEFC we found a decrease in the peak power density from 21.7 mW/cm^2 to 6.5 mW/cm^2 (- 70%) between the first linear sweep and the 0.2 V sweep. Formate FC (Figure 8-b) show a different trend, and identical power curves can be seen after the 0.4 V potentiostatic step. Here, for the DFFC, peak power density decreases of only 36% from 38.9 mW/cm^2 (1^{st} linear sweep) to 25.3 mW/cm^2 (0.4 V linear sweep). This result suggests degradation of the anodic catalyst in DFFC with a lower extent compared to the DEFC.

In Figure 9 the E vs time curves (black), coupled with the I vs time profiles (red) are reported. As expected, the DFFC exhibits greater performances, reaching higher current values at the same cell potential of DEFC. This is due to the ease with which potassium formate is fully oxidized to carbonate through a direct 2e- path [54]. Figure 9 shows that, for the EtOH FC, plateau current (current collected during galvanostatic steps) increases with the decrease of the potential between the two electrodes, from 0.6 V to 0.1 V. Different trend can be seen for the KCOOH FC. Below 0.4 V approximately same plateau end current is visible, but with increased in its slope during the potentiostatic stimulus.

Figure 10 shows the FC Open Circuit Potentials (OCPs) collected after each potentiostatic step step. From the figure, a smaller OCP variation can be seen regarding the initial value. Moreover, Open Circuit Potential variation seems to follow a similar pattern for both the DEFC and DFFC, suggesting a potential decrease phenomenon which is independent from the specific thermodynamics of the catalyst-fuel system.

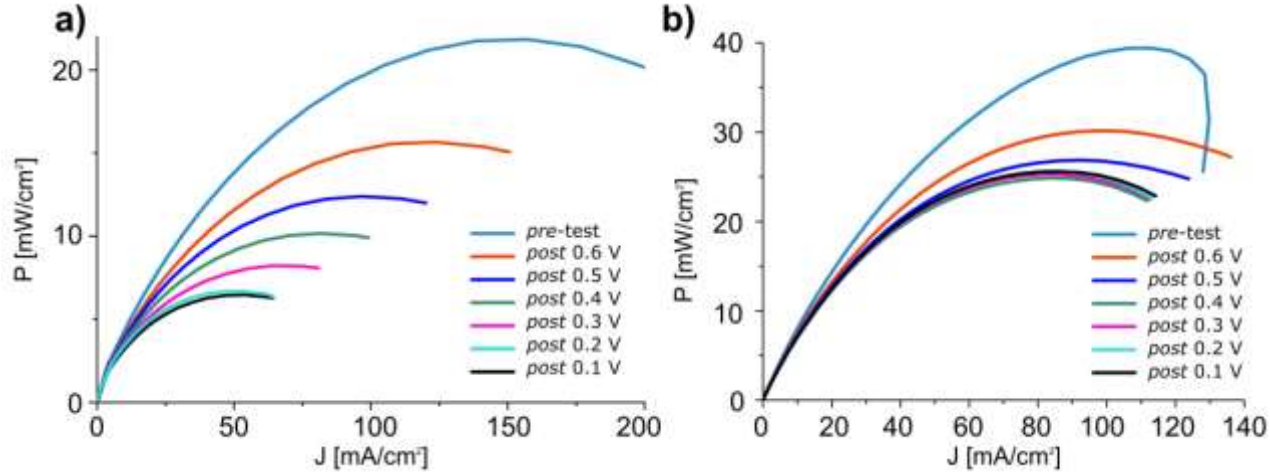

Figure 8 - Power curves acquired before (pre-test) and after each constant potential step (from 0.6 V to 0.1 V) for a) KOH 2 M + EtOH 2 M FC and b) KOH 2 M + KCOOH 2 M.

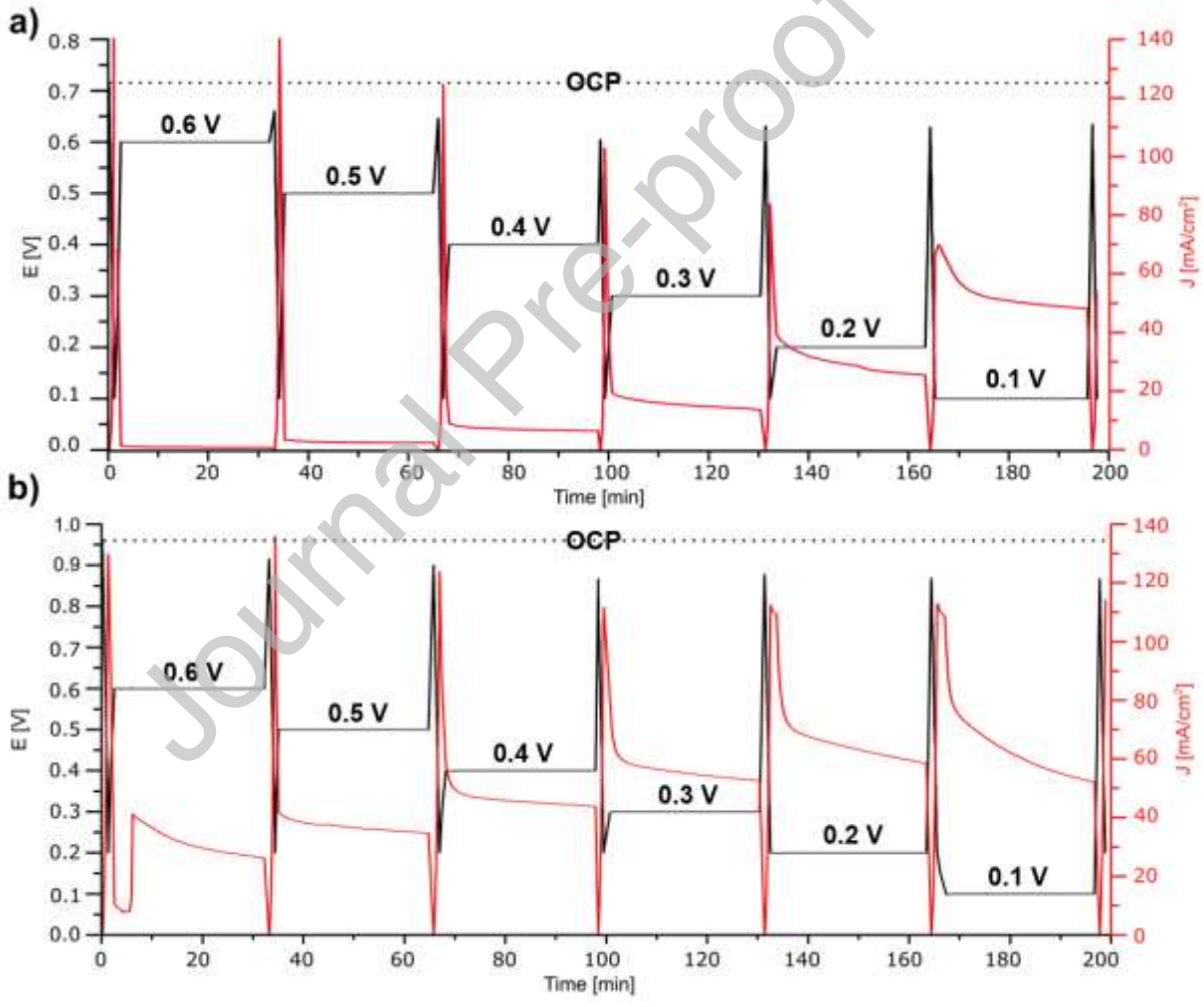

Figure 9 – E-time (black lines) and I-time (red lines) profiles for the potentiostatic tests on the DEFC (a, top row) and DFFC (b, bottom row). J was calculated by taking into account the geometrical average surface of the particles.

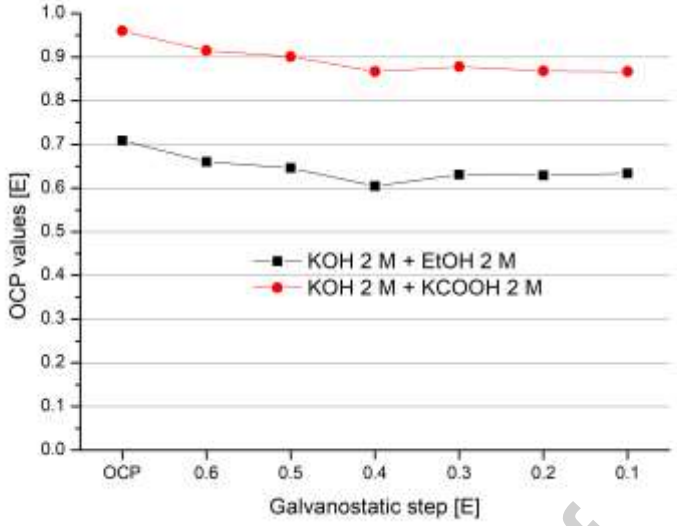

Figure 10 – OCP values collected after 1 minute from the galvanostatic steps

4. **Discussion**

Figure 11 (bottom row) shows that two different absorption coefficient trends occur for ethanol and formate FCs: 1) For the KOH 2 M + KCOOH 2 M electrolyte (Figure 11-d), no variation of μ_f and μ_1 between voltammetric cycles can be seen, 2) For the KOH 2 M + EtOH 2 M electrolyte (Figure 11-c), a linear decrease in the μ_f is detectable starting for the first voltametric cycle, changing its slope after the 6th voltametric cycle, thus following two distinct trends. For the DEFC, μ_f loss is in fact faster for the first part of the FEXRAV experiment, and slower for the second one, eventually reaching a steady horizontal state. Oppositely, a dependency can be seen considering μ_1 variation, which fastly increases for the first six cycles, and tends to smoothen up for the following ones. We observed similar trends during our previous FEXRAV half-cell experiments [46,47] performed using the same catalyst and fuel (Figure 11-b, top row). Here, we adopted disareated KOH 2 M + KOH 2 M electrolyte (Figure 11-b) in a three electrodes set-up, reaching higher oxidative potentials as voltammetry upper vertex (1.2 V vs. RHE).

The comparison between half-cell and fuel-cell experiments in EtOH solution confirms that similar deactivation phenomenon occurs, and thus that the main factor inducing performance loss is related to the anodic catalyst. Previous half-cell experiments in pure KOH 2M electrolytes showed a different trend (Figure 11-a). Here μ_f reported an almost monotonous decreasing trend, which seems to slightly change in slope only during the last FEXRAV cycles. We ascribe this fact to a possible decrease in the electroactive surface area due to the Pd nanoparticles dissolution. Figure 11 permits two important qualitative considerations. We relate the first one to the influence of the fuel on the dissolution of palladium, and the second one to the influence of the fuel on the fuel cell performances.

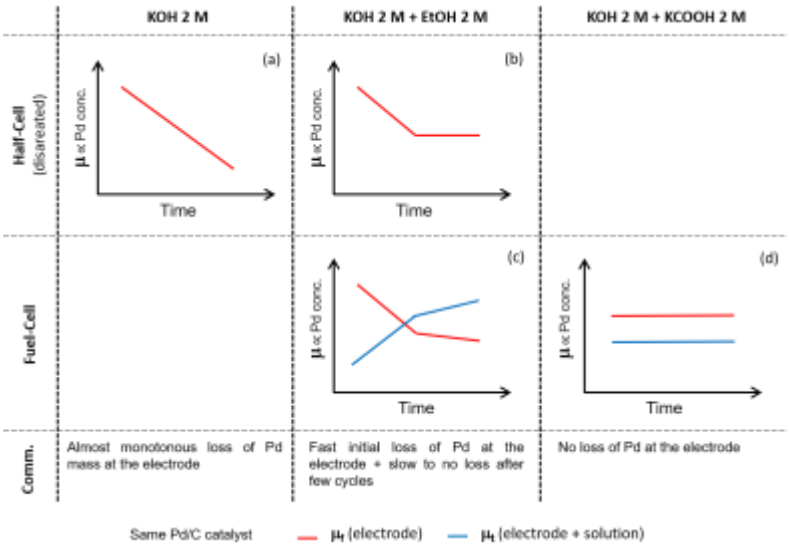

Figure 11 – Summary of the overall absorption coefficients ($\mu_{x,\ x=1,f}$) trends between the half-cell experiments ([46,47], top row) and the fuel-cell experiments (present article, bottom row)

4.1. Influence of the fuel on Pd dissolution

By considering that a decrease in the fluorescence absorption coefficient can be related to a loss of Pd mass at the electrode (as already stated in 3.1.) we can confirm that a) palladium subjected to anodic stimulus in KOH 2 M solution dissolves with the same rate when subjected to subsequent voltametric cycles, b) palladium subjected to anodic stimulus in KOH 2 M + EtOH 2 M incurs in an initial dissolution process, but having reached a certain particle dimension, the process slows down, eventually reaching a steady state (no dissolution, same trend is visible both for the half-cell experiments and for the FC experiments), and c) no Pd mass loss is visible during anodic stressing in KOH 2 M + KCOOH 2 M. This different behaviour can be justified by the nature of the fuels used. Both Ethanol and Formate possess different degrees of reducing capabilities in respect to Pd; EtOH is used to reduce Pd salts to nanoparticles during synthetic processes [55] being a milder reducing agent in respect to formate, which is adopted to recover metallic palladium from waste solutions at an industrial level [56]. Experimental evidence confirms this: the comparison between half-cell measurements reported in our previous work [46] suggested a faster Pd mass loss at the electrode for the KOH 2 M electrolyte in respect to the KOH 2 M + EtOH 2 M one. In the latter case a protective effect of the fuel due to reprecipitation/oxidation prevention could occur. For the DFFC mass loss is not evident at all, suggesting that formate plays a major role in the metallic palladium protection, not by avoiding its oxidation (μ variation in a single FEXRAV cycle is still visible), but by reprecipitating its dissolved compounds.

The palladium species we expect to be present in our system during the oxidation process are PdO (solid, at the electrode) and $Pd(OH)_4^{2-}$ (the dissolved form of Pd). These species were identified by our calculated Pd-O-H Pourbaix diagram [47], where Palladium hydroxylates were added according to the work of Mountain and Wood [57]. However, the presence of mainly Pd^{2+} species is in line with the results presented in works from other groups [58] for the same explored potential range. However, presence of PdO and $Pd(OH)_4^{2-}$ leads to a technical limitation. FEXRAV technique is able to follow the evolution of different Pd compounds during voltametric cycling at the working electrode. XAS, which is an element-sensitive technique, is capable of probing interactions between palladium and its first coordination shell in a fast and quantitative manner. Unfortunately, as stated in our previous articles on the topic ([46,47]), the species we expected from the calculated Pourbaix diagram give rise to similar XAS features. For this reason, FEXRAV alone cannot be used to qualify and quantify the amount of single Pd^{2+} species present both on the electrode and in solution.

4.2. Influence of the fuel on the FC performances

In both the analysed fuel cells it can be seen a certain degree of performance degradation in time. The continuous loss in DEFC performance is consistent with the palladium mass loss seen during FEXRAV experiments. It is possible to argue that in DEFCs the capping of the Pd electroactive surface by adsorbed/insoluble species plays a minor role in catalyst deactivation due to its dissolution. On the contrary, for DFFCs, a certain degree of FC performance loss is still visible, even if no dissolution of Pd was noticed during FEXRAV. Thus, for DFFCs, we can't exclude the occurrence of other catalyst degradation pathway (i.e. irreversible adsorption of species on the surface of the catalyst [39]). This suggests an initial deactivation process that is independent of the catalyst mass loss, and an increase in stability of the FC thanks to the reducing capabilities of the fuel [59].

A final consideration can be done in respect to Open Circuit Potentials values. The initial OCV is significantly higher for DFFC (0.960 V) compared with the DEFC (0.709 V). In both cells a decrease in OCV values is observed over time, until to -9.6 % in DFFC and -14.7% in DEFC. This phenomenon could be ascribed to the back-diffusion of water that results in cathode flooding, especially in lower current density region [60–62]. In the case of DFFC, current densities at high overpotential respect OCV (0.2 V and 0.1 V potentiostatic cycles) are similar; this is probably due to a diffusive control of the reaction and/or cathode limitations, since as seen from the power curves recorded between these two potentiostatic cycles, the performances remain unchanged. On the contrary, in the case of DEFC, ethanol oxidation is more difficult and it occurs only partially, through a 4e- path, leading to the formation of potassium acetate. Current densities of the order of 50 mA/cm2 are observed only at high overpotential (0.1 V potentiostatic cycle), but if we compare this current value with that of formate, this corresponds only to the oxidation of the half of the moles of ethanol.

5. **Conclusions**

Results showed unambiguously the dissolution of Pd under polarization cycles of DEFCs (KOH 2M + EtOH 2M). We proved this by in-situ in-operando X-Ray Absorption Voltammetry, by observing the decreasing trend of the fluorescence absorption signal (loss of Pd mass at the electrode) and the increasing trend of the transmitted signal (increase in Pd^{2+} content in solution). Pd mass loss in DEFC followed a similar (bimodal) trend in respect to our previous EtOH half-cell experiments, but different (monotonous) trend in respect to half-cell experiments performed using only KOH as electrolyte. Analogous FEXRAV experiments were performed using formate (KOH 2M + KCOOH 2M), a fuel with higher reducing capabilities, showing a steady-state for both the absorption signals. This suggested no Pd dissolution in the timespan of the experiments, even during dynamic potential cycling between DFFC OCP and 0.1 V. To exclude purely chemical influence on the dissolution phenomenon, we acquired XANES spectra of the Pd/C catalyst at the OCP, in contact with the two fuel solutions. On a 5 hours' test, no variation in absorption coefficient above the method's sensitivity was noticeable, confirming the stability of the catalyst in a non-working, purely chemical situation. Power density curves acquired after potential steps at increasing cell polarization showed performance degradation trends between ethanol and formate fuels. Mainly, DEFCs degrade heavier compared to DFFC. We argue that the different palladium dissolution trends in the two systems may play a significant role in FCs loss in performance.

Acknowledgements:

Authors wanted to acknowledge Italian National Research MIUR project “Nuovi elettrodi nanostrutturati, multistrato e micro-lavorati per applicazioni elettrocatalitiche (celle a combustibile ed elettrolizzatori)” (PRIN 2017 cod. 2017YH9MRK) and Tuscany Regional project “Fotonica ed Elettronica Integrate per l’industria” (Regione Toscana - Por CREO FESR 2014-2020 proj. cod. n. DD 5262 del 09/11/2015) for financial support.

Declaration of interests

☒ The authors declare that they have no known competing financial interests or personal relationships that could have appeared to influence the work reported in this paper.

Credit Author Statement:

E.Berretti: Investigation, Writing - Original Draft, Writing - Revised Draft, Visualization **M. V. Pagliaro:** Investigation, Writing - Original Draft, Writing - Revised Draft **A.Giaccherini:** Investigation, Visualization, **G.Montegrossi:** Investigation, Methodology **F.Di Benedetto:** Investigation, Methodology, Validation **G.O. Lepore:** Investigation **F. D'Acapito:** Investigation, Methodology **F. Vizza:** Resources, Supervision **A. Lavacchi:** Conceptualization, Methodology, Validation, Supervision

6. Bibliography

[1] H.R. Corti, E.R. Gonzalez, eds., Direct Alcohol Fuel Cells, Springer Netherlands, Dordrecht, 2014. https://doi.org/10.1007/978-94-007-7708-8.

[2] M.A. Damin Zhanga, Jia Dua, Jonathan Quinsonb, On the electro-oxidation of small organic molecules: towards a fuel cell catalyst testing platform with realistic reaction environment Damin Zhang, ChemXiv. (n.d.) 1–24.

[3] D.M. Fadzillah, S.K. Kamarudin, M.A. Zainoodin, M.S. Masdar, Critical challenges in the system development of direct alcohol fuel cells as portable power supplies: An overview, Int. J. Hydrogen Energy. 44 (2019) 3031–3054. https://doi.org/10.1016/j.ijhydene.2018.11.089.

[4] Y. Chen, M. Bellini, M. Bevilacqua, P. Fornasiero, A. Lavacchi, H.A. Miller, L. Wang, F. Vizza, Direct Alcohol Fuel Cells: Toward the Power Densities of Hydrogen-Fed Proton Exchange Membrane Fuel Cells, ChemSusChem. 8 (2015) 524–533. https://doi.org/10.1002/cssc.201402999.

[5] A.B.F. Dalena, Alcohols and bioalcohols : characteristics, production, and uses, New York, NY, 2014.

[6] H.A. Miller, A. Lavacchi, F. Vizza, Storage of renewable energy in fuels and chemicals through electrochemical reforming of bioalcohols, Curr. Opin. Electrochem. 21 (2020) 140–145. https://doi.org/10.1016/j.coelec.2020.02.001.

[7] Z.M. Bhat, R. Thimmappa, N.C. Dargily, A. Raafik, A.R. Kottaichamy, M.C. Devendrachari, M. Itagi, H.M.N. Kotresh, S.A. Freunberger, M.O. Thotiyl, Ambient Condition Alcohol Reforming to Hydrogen with Electricity Output, ACS Sustain. Chem. Eng. 9 (2021) 3104–3111. https://doi.org/10.1021/acssuschemeng.0c07547.

[8] Direct Alcohol Fuel Cells for Portable Applications, Elsevier, 2018. https://doi.org/10.1016/C2016-0-00632-0.

[9] T.S. Zhao, R. Chen, W.W. Yang, C. Xu, Small direct methanol fuel cells with passive supply of reactants, J. Power Sources. 191 (2009) 185–202. https://doi.org/10.1016/j.jpowsour.2009.02.033.

[10] A.M. Sheikh, K. Ebn-Alwaled Abd-Alftah, C.F. Malfatti, On reviewing the catalyst materials for direct

alcohol fuel cells (DAFCs), J. Multidiscip. Eng. Sci. Technol. 1 (2014) 3159–40.

[11] Y. Wang, S. Zou, W.-B. Cai, Recent Advances on Electro-Oxidation of Ethanol on Pt- and Pd-Based Catalysts: From Reaction Mechanisms to Catalytic Materials, Catalysts. (2015). https://doi.org/10.3390/catal5031507.

[12] A. Yuda, A. Ashok, A. Kumar, A comprehensive and critical review on recent progress in anode catalyst for methanol oxidation reaction, (2020).

[13] L. An, R. Chen, Direct formate fuel cells : A review, 320 (2016). https://doi.org/10.1016/j.jpowsour.2016.04.082.

[14] X. Su, Z. Pan, L. An, Performance characteristics of a passive direct formate fuel cell, (2019) 1–11. https://doi.org/10.1002/er.4775.

[15] H.A. Miller, F. Vizza, A. Lavacchi, Direct Alcohol Fuel Cells: Nanostructured Materials for the Electrooxidation of Alcohols in Alkaline Media, in: 2016: pp. 477–516. https://doi.org/10.1007/978-3-319-29930-3_12.

[16] J.M. Leger, C. Coutanceau, C. Lamy, Electrocatalysis for the Direct Alcohol Fuel Cell, Fuel Cell Catal. A Surf. Sci. Approach. (2008) 343–373. https://doi.org/10.1002/9780470463772.ch11.

[17] K.I. Ozoemena, Nanostructured platinum-free electrocatalysts in alkaline direct alcohol fuel cells: catalyst design, principles and applications, RSC Adv. 6 (2016) 89523–89550. https://doi.org/10.1039/C6RA15057H.

[18] E. Berretti, M. Longhi, P. Atanassov, D. Sebastián, C. Lo Vecchio, V. Baglio, A. Serov, A. Marchionni, F. Vizza, C. Santoro, A. Lavacchi, Platinum group metal-free Fe-based (Fe N C) oxygen reduction electrocatalysts for direct alcohol fuel cells, Curr. Opin. Electrochem. 29 (2021) 100756. https://doi.org/10.1016/j.coelec.2021.100756.

[19] C. Lamy, A. Lima, V. LeRhun, F. Delime, C. Coutanceau, J.M. Léger, Recent advances in the development of direct alcohol fuel cells (DAFC), J. Power Sources. 105 (2002) 283–296. https://doi.org/10.1016/S0378-7753(01)00954-5.

[20] H. Liu, C. Song, L. Zhang, J. Zhang, H. Wang, D.P. Wilkinson, A review of anode catalysis in the direct methanol fuel cell, J. Power Sources. 155 (2006) 95–110. https://doi.org/10.1016/j.jpowsour.2006.01.030.

[21] T. Huang, J. Liu, R. Li, W. Cai, A. Yu, A novel route for preparation of PtRuMe (Me=Fe, Co, Ni) and their catalytic performance for methanol electrooxidation, Electrochem. Commun. 11 (2009) 643–646. https://doi.org/10.1016/j.elecom.2009.01.008.

[22] Z.-B. Wang, P.-J. Zuo, G.-P. Yin, Investigations of Compositions and Performance of PtRuMo/C Ternary Catalysts for Methanol Electrooxidation, Fuel Cells. 9 (2009) 106–113. https://doi.org/10.1002/fuce.200800096.

[23] M.E. Scofield, C. Koenigsmann, L. Wang, H. Liu, S.S. Wong, Tailoring the composition of ultrathin, ternary alloy PtRuFe nanowires for the methanol oxidation reaction and formic acid oxidation reaction, Energy Environ. Sci. 8 (2015) 350–363. https://doi.org/10.1039/C4EE02162B.

[24] A.O. Neto, E.G. Franco, E. Aricó, M. Linardi, New Electrocatalysts for Electro-Oxidation of Methanol Prepared by Bönnemann´s Method, Port. Electrochim. Acta. 22 (2004) 93–101. https://doi.org/10.4152/pea.200402093.

[25] S. Pasupathi, V. Tricoli, Effect of third metal on the electrocatalytic activity of PtRu/Vulcan for methanol electro-oxidation, J. Solid State Electrochem. 12 (2008) 1093–1100. https://doi.org/10.1007/s10008-007-0441-y.

[26] T. Maiyalagan, B. Viswanathan, Catalytic activity of platinum/tungsten oxide nanorod electrodes towards electro-oxidation of methanol, J. Power Sources. 175 (2008) 789–793. https://doi.org/10.1016/j.jpowsour.2007.09.106.

[27] T. Maiyalagan, F.N. Khan, Electrochemical oxidation of methanol on Pt/V2O5–C composite catalysts, Catal. Commun. 10 (2009) 433–436. https://doi.org/10.1016/j.catcom.2008.10.011.

[28] C. Zhou, H. Wang, F. Peng, J. Liang, H. Yu, J. Yang, MnO 2 /CNT Supported Pt and PtRu Nanocatalysts for Direct Methanol Fuel Cells, Langmuir. 25 (2009) 7711–7717. https://doi.org/10.1021/la900250w.

[29] L. Ma, D. Chu, R. Chen, Comparison of ethanol electro-oxidation on Pt/C and Pd/C catalysts in alkaline media, Int. J. Hydrogen Energy. 37 (2012) 11185–11194. https://doi.org/10.1016/j.ijhydene.2012.04.132.

[30] C. Bianchini, P.K. Shen, Palladium-based electrocatalysts for alcohol oxidation in half cells and in direct alcohol fuel cells, Chem. Rev. 109 (2009) 4183–4206. https://doi.org/10.1021/cr9000995.

[31] V. Bambagioni, C. Bianchini, Y. Chen, J. Filippi, P. Fornasiero, M. Innocenti, A. Lavacchi, A. Marchionni, W. Oberhauser, F. Vizza, Energy Efficiency Enhancement of Ethanol Electrooxidation on Pd–CeO 2 /C in Passive and Active Polymer Electrolyte-Membrane Fuel Cells, ChemSusChem. 5 (2012) 1266–1273. https://doi.org/10.1002/cssc.201100738.

[32] H.A. Miller, A. Lavacchi, F. Vizza, M. Marelli, F. Di Benedetto, F. D'Acapito, Y. Paska, M. Page, D.R. Dekel, A Pd/C-CeO 2 Anode Catalyst for High-Performance Platinum-Free Anion Exchange Membrane Fuel Cells, Angew. Chemie Int. Ed. 55 (2016) 6004–6007. https://doi.org/10.1002/anie.201600647.

[33] L.K. Tsui, C. Zafferoni, A. Lavacchi, M. Innocenti, F. Vizza, G. Zangari, Electrocatalytic activity and operational stability of electrodeposited Pd-Co films towards ethanol oxidation in alkaline electrolytes, J. Power Sources. (2015). https://doi.org/10.1016/j.jpowsour.2015.05.121.

[34] R. STEINBERGER-WILCKENS, J. MERGEL, A. GLÜSEN, K. WIPPERMANN, I. VINKE, P. BATFALSKY, M.J. SMITH, Performance degradation and failure mechanisms of fuel cell materials, in: Mater. Fuel Cells, Elsevier, 2008: pp. 425–465. https://doi.org/10.1533/9781845694838.425.

[35] L. Wang, A. Lavacchi, M. Bellini, F. D'Acapito, F. Di Benedetto, M. Innocenti, H.A. Miller, G. Montegrossi, C. Zafferoni, F. Vizza, Deactivation of Palladium Electrocatalysts for Alcohols Oxidation in Basic Electrolytes, Electrochim. Acta. (2015). https://doi.org/10.1016/j.electacta.2015.02.026.

[36] E. Antolini, E.R. Gonzalez, Alkaline direct alcohol fuel cells, J. Power Sources. 195 (2010) 3431–3450. https://doi.org/10.1016/j.jpowsour.2009.11.145.

[37] Y.S. Li, T.S. Zhao, Understanding the performance degradation of anion-exchange membrane direct ethanol fuel cells, 7 (2011). https://doi.org/10.1016/j.ijhydene.2011.11.086.

[38] W. Huang, X. Ma, H. Wang, R. Feng, J. Zhou, P.N. Duchesne, Promoting Effect of Ni (OH) 2 on Palladium Nanocrystals Leads to Greatly Improved Operation Durability for Electrocatalytic Ethanol Oxidation in Alkaline Solution, 1703057 (2017) 1–8. https://doi.org/10.1002/adma.201703057.

[39] M. Ren, Y. Kang, W. He, Z. Zou, X. Xue, D.L. Akins, H. Yang, S. Feng, Applied Catalysis B : Environmental Origin of performance degradation of palladium-based direct formic acid fuel cells, "Applied Catal. B, Environ. 104 (2011) 49–53. https://doi.org/10.1016/j.apcatb.2011.02.029.

[40] Z. Wu, B. Miao, E. Hopkins, K. Park, Y. Chen, H. Jiang, M. Zhang, C. Zhong, L. Wang, Poisonous Species in Complete Ethanol Oxidation Reaction on Palladium Catalysts, (n.d.). https://doi.org/10.1021/acs.jpcc.9b04229.

[41] J. Wang, N. Cheng, M.N. Banis, B. Xiao, A. Riese, X. Sun, Comparative study to understand the intrinsic properties of Pt and Pd catalysts for methanol and ethanol oxidation in alkaline media,

Electrochim. Acta. 185 (2015) 267–275. https://doi.org/10.1016/j.electacta.2015.10.151.

[42] S. Kabir, A. Zadick, P. Atanassov, L. Dubau, M. Chatenet, Stability of carbon-supported palladium nanoparticles in alkaline media: A case study of graphitized and more amorphous supports, Electrochem. Commun. (2017). https://doi.org/10.1016/j.elecom.2017.03.017.

[43] M. Grdeń, M. Łukaszewski, G. Jerkiewicz, A. Czerwiński, Electrochemical behaviour of palladium electrode: Oxidation, electrodissolution and ionic adsorption, Electrochim. Acta. 53 (2008) 7583–7598. https://doi.org/10.1016/j.electacta.2008.05.046.

[44] H.A. Miller, L. Wang, M. Bellini, J. Filippi, A. Marchionni, M.G. Folliero, A. Lavacchi, M. V. Pagliaro, F. Vizza, Performance Evaluation of a Platinum-Free Microscale Alkaline Direct Ethanol Fuel Cell Operating for Long Periods, Energy Technol. 4 (2016) 1119–1124. https://doi.org/10.1002/ente.201600143.

[45] J.C.C. Gómez, R. Moliner, M.J. Lázaro, Palladium-based catalysts as electrodes for direct methanol fuel cells: A last ten years review, Catalysts. 6 (2016). https://doi.org/10.3390/catal6090130.

[46] Berretti, Giaccherini, Montegrossi, D'Acapito, Di Benedetto, Zafferoni, Puri, Lepore, Miller, Giurlani, Innocenti, Vizza, Lavacchi, In-situ Quantification of Nanoparticles Oxidation: A Fixed Energy X-ray Absorption Approach, Catalysts. 9 (2019) 659. https://doi.org/10.3390/catal9080659.

[47] G. Montegrossi, A. Giaccherini, E. Berretti, F. Di Benedetto, M. Innocenti, F. D'Acapito, A. Lavacchi, Computational Speciation Models: A Tool for the Interpretation of Spectroelectrochemistry for Catalytic Layers under Operative Conditions, J. Electrochem. Soc. 164 (2017) E3690–E3695. https://doi.org/10.1149/2.0711711jes.

[48] A. Minguzzi, O. Lugaresi, C. Locatelli, S. Rondinini, F. D'Acapito, E. Achilli, P. Ghigna, Fixed energy X-ray absorption voltammetry, Anal. Chem. 85 (2013) 7009–7013. https://doi.org/10.1021/ac401414v.

[49] A.P. Francesco d'Acapito, Giovanni Orazio Lepore, A.D.L. Alessio Laloni, Fabrizio La Manna, Eric Dettona, A. Martin, The LISA beamline at ESRF, (2019) 551–558. https://doi.org/10.1107/S160057751801843X.

[50] A. Puri, G. Lepore, F. D'Acapito, The New Beamline LISA at ESRF: Performances and Perspectives for Earth and Environmental Sciences, Condens. Matter. 4 (2019) 12. https://doi.org/10.3390/condmat4010012.

[51] B. Ravel, M. Newville, ATHENA, ARTEMIS, HEPHAESTUS: Data analysis for X-ray absorption spectroscopy using IFEFFIT, J. Synchrotron Radiat. 12 (2005) 537–541. https://doi.org/10.1107/S0909049505012719.

[52] H. Miller, J. Ruggeri, A. Marchionni, M. Bellini, M. Pagliaro, C. Bartoli, A. Pucci, E. Passaglia, F. Vizza, Improving the Energy Efficiency of Direct Formate Fuel Cells with a Pd/C-CeO2 Anode Catalyst and Anion Exchange Ionomer in the Catalyst Layer, Energies. 11 (2018) 369. https://doi.org/10.3390/en11020369.

[53] V. Bambagioni, C. Bianchini, J. Filippi, A. Lavacchi, W. Oberhauser, A. Marchionni, S. Moneti, F. Vizza, R. Psaro, V. Dal Santo, A. Gallo, S. Recchia, L. Sordelli, Single-site and nanosized Fe–Co electrocatalysts for oxygen reduction: Synthesis, characterization and catalytic performance, J. Power Sources. 196 (2011) 2519–2529. https://doi.org/10.1016/j.jpowsour.2010.11.030.

[54] M.V. Pagliaro, M. Bellini, J. Filippi, M.G. Folliero, A. Marchionni, H.A. Miller, W. Oberhauser, F. Vizza, Hydrogen production from the electrooxidation of methanol and potassium formate in alkaline media on carbon supported Rh and Pd nanoparticles, Inorganica Chim. Acta. 470 (2018) 263–269. https://doi.org/10.1016/j.ica.2017.05.055.

[55] J. Cookson, The Preparation of Palladium Nanoparticles, Platin. Met. Rev. 56 (2012) 83–98.

https://doi.org/10.1595/147106712X632415.

[56] G. Prabaharan, S.P. Barik, B. Kumar, A hydrometallurgical process for recovering total metal values from waste monolithic ceramic capacitors, Waste Manag. 52 (2016) 302–308. https://doi.org/10.1016/j.wasman.2016.04.010.

[57] B.W. Mountain, S.A. Wood, Chemical controls on the solubility, transport and deposition of platinum and palladium in hydrothermal solutions; a thermodynamic approach, Econ. Geol. 83 (1988) 492–510. https://doi.org/10.2113/gsecongeo.83.3.492.

[58] M. Schalenbach, O. Kasian, M. Ledendecker, F.D. Speck, A.M. Mingers, K.J.J. Mayrhofer, S. Cherevko, The Electrochemical Dissolution of Noble Metals in Alkaline Media, Electrocatalysis. 9 (2018) 153–161. https://doi.org/10.1007/s12678-017-0438-y.

[59] L. Wang, V. Bambagioni, M. Bevilacqua, C. Bianchini, J. Filippi, A. Lavacchi, A. Marchionni, F. Vizza, X. Fang, P.K. Shen, Sodium borohydride as an additive to enhance the performance of direct ethanol fuel cells, J. Power Sources. 195 (2010) 8036–8043. https://doi.org/10.1016/j.jpowsour.2010.06.101.

[60] S. Song, W. Zhou, J. Tian, R. Cai, G. Sun, Q. Xin, S. Kontou, P. Tsiakaras, Ethanol crossover phenomena and its influence on the performance of DEFC, J. Power Sources. 145 (2005) 266–271. https://doi.org/10.1016/j.jpowsour.2004.12.065.

[61] N. Park, T. Shiraishi, K. Kamisugi, Y. Hara, K. Iizuka, T. Kado, S. Hayase, NiCoFe/C cathode electrocatalysts for direct ethanol fuel cells, J. Appl. Electrochem. 38 (2008) 371–375. https://doi.org/10.1007/s10800-007-9445-7.

[62] E.A. Monyoncho, T.K. Woo, E.A. Baranova, Ethanol electrooxidation reaction in alkaline media for direct ethanol fuel cells, in: n.d.: pp. 1–57. https://doi.org/10.1039/9781788013895-00001.